Modeling Buffered Ca^{2+} Diffusion Near the Membrane: Implications for Secretion in Neuroendocrine Cells

Jürgen Klingauf and Erwin Neher
Department of Membrane Biophysics, Max-Planck-Institute for Biophysical Chemistry, Am Fassberg, D-37077 Göttingen, Germany

ABSTRACT Secretion of catecholamines from neuroendocrine cells is relatively slow and it is likely that redistribution and buffering of Ca^{2+} is a major factor for delaying the response after a stimulus. In fact, in a recent study (Chow, R. H., J. Klingauf, and E. Neher. 1994. Time course of Ca^{2+} concentration triggering exocytosis in neuroendocrine cells. *Proc. Natl. Acad. Sci. U.S.A.* 91:12765–12769) Chow et al. concluded that the concentration of free calcium ($[Ca^{2+}]_i$) at a release site peaks at <10 μM during short-step depolarizations, and then decays to baseline over tens of milliseconds. To check whether such a time course is consistent with diffusion theory, we modeled buffered diffusion in the vicinity of a Ca^{2+} channel pore. Peak $[Ca^{2+}]_i$ and the slow decay were well simulated when release-ready granules were randomly distributed within a regular grid of Ca^{2+} channels with mean interchannel distances of 300–600 nm. For such large spacings, however, the initial rise in $[Ca^{2+}]_i$ was underestimated, suggesting that a small fraction of the release-ready pool (~10%) experiences much higher $[Ca^{2+}]_i$, and thus might be collocalized with Ca^{2+} channels. A model that accommodates these findings then correctly predicts many recent observations, including the result that single action potentials evoke near-synchronous transmitter release with low quantal yield, whereas trains of action potentials lead to desynchronized release, but with severalfold increased quantal yield. The simulations emphasize the role of Ca^{2+} not only in triggering, but also in modulating the secretory response: buffers are locally depleted by residual Ca^{2+} of a preceding stimulus, so that a second pulse leads to a larger peak $[Ca^{2+}]_i$ at the fusion sites.

INTRODUCTION

In synapses, Ca^{2+}-triggered secretion of neurotransmitters is fast, i.e., most release events occur within a millisecond after arrival of an action potential (Augustine et al., 1985). The delay between the entrance of Ca^{2+} through voltage-activated Ca^{2+} channels and the onset of a postsynaptic response has been measured to ~200 μs (Llinas et al., 1981), which sets an upper bound for the time required by Ca^{2+} ions to diffuse to the fusogenic receptor. Thus, investigators have speculated that Ca^{2+} channels and fusion sites are in close proximity, being only some tens of nanometers apart. Theoretical considerations led to the view that regions of elevated $[Ca^{2+}]_i$, so-called *microdomains*, which are formed around an open Ca^{2+} channel, are responsible for the synchronization of vesicle fusion with an action potential. Several modeling studies showed that the $[Ca^{2+}]_i$ dynamics of these microdomains meet the requirements for triggering fast secretion (Chad and Eckert, 1984; Simon and Llinas, 1985; Fogelson and Zucker, 1985; Parnas et al., 1989; Yamada and Zucker, 1992). Microdomains build up within microseconds, which can account for the speed of the secretory response. Within microdomains $[Ca^{2+}]_i$ reaches steady state concentrations of several tens of micromoles per liter, a prerequisite for the activation of the high-threshold receptor (von Gersdorff and Matthews, 1994; Heidelberger et al., 1994). Finally, the fast dissipation of microdomains after channel closing assures a fast cessation of most of the secretory response, i.e., it guarantees synchronization.

In chromaffin cells, in contrast, Chow et al. (1992), using carbon fibers to monitor secretion electrochemically, could show that secretion continues for tens of milliseconds after the end of short-step depolarizations. This is surprising, if $[Ca^{2+}]_i$ domains around channels trigger secretion, since they dissipate in <100 μs (Roberts, 1994; Yamada and Zucker, 1992). A small proportion of transmitter, however, is released more asynchronously, and with long latencies at the neuromuscular junction (Rahamimoff and Yaari, 1973) and hippocampal synapses (Goda and Stevens, 1994); displaying release kinetics similar to those found in neuroendocrine cells. Two explanations have been given for these findings: the existence of two types of Ca^{2+}-triggered secretion, fast and slow, mediated by different types of Ca^{2+} receptors and fusogenic proteins (Goda and Stevens, 1994); or else slow cessation of the "residual" $[Ca^{2+}]_i$ signal during delayed release after collapse of microdomains (Rahamimoff and Yaari, 1973). By extrapolation one could speculate that in neuroendocrine cells either the Ca^{2+} receptor and fusion machinery are of the "slow" type, or that the $[Ca^{2+}]_i$ signal is different from that in synapses, i.e., that microdomains are not relevant for triggering secretion.

Experimentally, these issues are difficult to resolve, since the limited spatial and temporal resolution of ratiometric imaging methods still prevents direct measurement of the submembrane $[Ca^{2+}]_i$ at the sites of secretion. Thus, experimental evidence is rather indirect. In synapses exogenous Ca^{2+} buffers have little effect on the size and shape of the secretory response (Adler et al., 1991), in agreement with theoretical predictions based on the microdomain hypothe-

Received for publication 19 August 1996 and in final form 23 October 1996.

Address reprint requests to Dr. Erwin Neher, Dept. of Membrane Biophysics, Max-Planck-Institute for Biophysical Chemistry, Am Fassberg, D-37077 Göttingen, Germany. Tel.: 49-551-2011675; Fax: 49-551-2011688; E-mail: eneher@gwdg.de.

0006-3495/97/02/674/17 $2.00

sis. In contrast, Ca^{2+} chelators interfere with the time course of secretion in bovine chromaffin cells (Chow et al., 1996), which suggests, that the "slowness" of secretion in these cells is determined by a slow $[Ca^{2+}]_i$ transient. In previous work we addressed these issues experimentally in neuroendocrine cells using flash photolysis: the secretion response was analyzed upon perturbation of the steady-state $[Ca^{2+}]_i$ in a step-like fashion by photolysing Ca^{2+}-loaded DM-nitrophen (Neher and Zucker, 1993; Thomas et al., 1993; Heinemann et al., 1994). By using these methods we suggested a kinetic model for the final steps in secretion and determined the rate constants for Ca^{2+} binding and unbinding (Heinemann et al., 1994). It was concluded that in chromaffin cells the relaxation of the Ca^{2+}-binding and fusion reaction should contribute only 1–2 ms to the slow decay of secretion upon short depolarizations. In another study we addressed the contribution of the release process after fusion of a vesicle and found that release of catecholamines follows fusion within a few milliseconds and, thus, does not contribute significantly to the slowness of secretion in neuroendocrine cells (Chow et al., 1996). The kinetic model derived from flash data was used to infer the time dependency of $[Ca^{2+}]_i$ at the release sites from rates of release measured during short step depolarizations (Chow et al., 1994). This "back-calculated" time course resembled $[Ca^{2+}]_i$ transients as predicted by conventional shell models (Sala and Hernández-Cruz, 1990; Nowycky and Pinter, 1993), which is in agreement with the hypothesis that slow $[Ca^{2+}]_i$ dynamics are responsible for the long secretory latencies in these cells.

In this study we further investigate the role of Ca^{2+} diffusion and redistribution in the secretion process in the context of the above findings. We model buffered Ca^{2+} diffusion in the vicinity of channels and release sites based on experimental estimates of cellular Ca^{2+} buffers (Zhou and Neher, 1993), and we find that our experimental data are most compatible with the assumption that the majority of vesicles is docked at a distance of ~200-300 nm from the nearest Ca^{2+} channel.

METHODS

Buffered diffusion

Complexation of Ca^{2+} by a buffer species X is modeled by a simple second-order process with the apparent rate constants k_x^+ and k_x^- for the forward and the backward reaction, respectively:

$$B_X + Ca^{2+} \underset{k_X^-}{\overset{k_X^+}{\rightleftharpoons}} Ca^{2+}B_X \qquad (1)$$

The apparent rate constants account for the fact that part of the buffer molecules may be protonated or bound to Mg^{2+} (cf. Neher, 1986, for a detailed discussion).

If second-order kinetics for Ca^{2+} buffer interaction, and Fickian diffusion for all diffusing species are assumed, then buffered diffusion in the cytoplasm is described by the following system of transport equations:

$$\begin{aligned}\frac{\partial}{\partial t}[Ca^{2+}] &= D_{Ca}\Delta[Ca^{2+}] \qquad (2)\\ &\quad - \sum_m\{k_m^+[Ca^{2+}][B_m] - k_m^-([B_m^{total}] - [B_m])\}\\ &\quad - \sum_f\{k_f^+[Ca^{2+}][B_f] - k_f^-([B_f^{total}] - [B_f])\}\frac{\partial}{\partial t}[B_m]\\ &= D_{B_m}\Delta[B_m] - k_m^+[Ca^{2+}][B_m] + k_m^-([B_m^{total}]\\ &\quad - [B_m])\frac{\partial}{\partial t}[Ca^{2+}B_f]\\ &= k_f^+[Ca^{2+}][B_f] - k_f^-([B_f^{total}] - [B_f])\end{aligned}$$

where square brackets denote concentration, D_X the diffusion constants of species X. Several species of mobile buffers, B_m, and fixed buffers, B_f, respectively, are considered. The Laplacian operator is Δ. For simplicity, the same diffusion constant is assumed for both the free and the complexed form of a given buffer species.

Microdomain model

For what follows, we have to define some boundary and initial conditions for the case of depolarization-induced calcium signals. Since there are no signs of "calcium-induced calcium release" from internal stores in response to single depolarizations up to 2 s (Neher and Augustine, 1992), Ca^{2+} is assumed to enter the cytosol only through voltage-activated Ca^{2+} channels.

Although studied intensively (Carmichael, 1987) no correlate to synaptic active zones was found in chromaffin cells. Hence, for simplicity we assume uniform distribution of N_{ch} Ca^{2+} channels at the surface of the spherical chromaffin cell (O'Sullivan et al., 1989; Neher and Augustine, 1992; but see Monck et al., 1994, and Schroeder et al., 1994, for discussion of the possibility of channel clustering).

The modeling of buffered diffusion for the case of Ca^{2+} entry through channel pores is severely complicated by two properties of the steep $[Ca^{2+}]_i$ gradients (microdomains) in the vicinity of a channel's mouth: firstly, microdomains build up and dissipate within microseconds (Roberts, 1994), so that the $[Ca^{2+}]_i$ time course near the pore follows closely the opening and closing ("flickering") of the channel; secondly, these events are stochastic such that microdomains from adjacent channels will overlap in a complicated fashion depending on the distance in-between and the duration of openings (Roberts, 1994). Because we are interested here only in those aspects of submembrane $[Ca^{2+}]_i$ time course that determine secretion, we first investigate the impact of flickering microdomains on the latter. This will be helpful later to simplify the model representation of buffered diffusion.

Low-pass properties of the Ca^{2+} sensor

Based on the analysis of secretion responses in bovine chromaffin cells after flash photolysis of caged Ca^{2+}, Heinemann et al. (1994) suggested a kinetic model, which faithfully predicts the time course of secretion in response to step changes in $[Ca^{2+}]_i$ over three orders of magnitude. Given the rate constants of this model, one can explore the impact of Ca^{2+} channel flickering on the probability of release for the case that the release sites are located next to channel pores. In this case the Ca^{2+} concentration profile should be approximately rectangular with a peak concentration of several tens of micromolar (Roberts, 1994). Fig. 1 shows the predicted secretory responses to a rectangular $[Ca^{2+}]_i$ signal with varying frequency, but constant total time integral. The amount of secretion is maximal at small frequencies and decreases with higher frequencies. It reaches a plateau at ~200 Hz, which is ~97.3% of the maximum for a $[Ca^{2+}]_i$

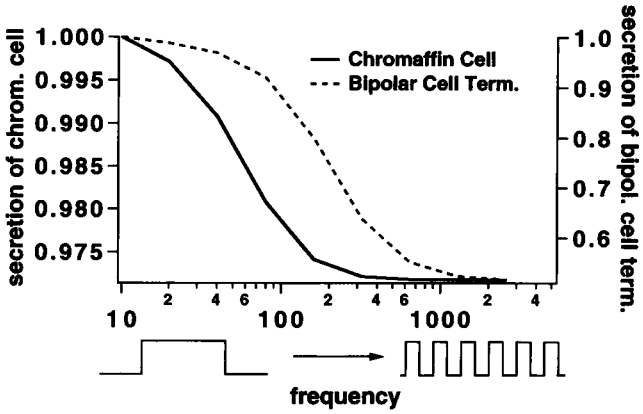

FIGURE 1 Secretion as a low-pass filter of Ca^{2+} channel flickering. Plotted are simulated relative responses of secretion for an idealized $[Ca^{2+}]_i$ time course close to a flickering Ca^{2+} channel. For each data point, secretion during a total of 50 ms of channel opening was calculated. This 50 ms of influx was subdivided into a pulse train with a frequency as given by the abscissa. For simplicity the channel is assumed to flicker with constant frequency during that period. The $[Ca^{2+}]_i$ around the channel pore follows instantly, resulting in a rectangular wave 30 μM in amplitude. The hypothetical chromaffin cell response is calculated according to Eq. 12; the response of a bipolar cell terminal was calculated using the kinetic scheme suggested by Heidelberger et al. (1994). In brief, four sequential cooperative Ca^{2+}-binding steps were assumed, with a binding rate constant of $14 \times 10^6\ M^{-1}s^{-1}$ for all steps. Cooperativity was introduced by scaling the dissociation rate of 2000 s^{-1} for the first step with a factor of 0.4 for the next step, and 0.4^2 and 0.4^3 for subsequent steps, respectively. The final secretion rate was set to 3000 s^{-1}, and the initial vesicle pool to 77 fF. To avoid depletion, the pool of docked vesicles was held constant in the simulations.

amplitude of 30 μM, and is identical to the secretory response elicited by a constant $[Ca^{2+}]_i$ of mean magnitude. The mean open time of a single Ca^{2+} channel in chromaffin cells is only ~1 ms (Fenwick et al., 1982). Thus, for studying the $[Ca^{2+}]_i$ dynamics underlying secretion, we can neglect the channel flickering during longer depolarizations and model a channel simply as flux with an amplitude given by the mean single channel current averaged over the pulse duration. Fig. 1 also shows the results of the same calculation performed with kinetic parameters as measured in a neuronal terminal. In this case secretion is quite strongly dependent on the frequency of stimulation. Nevertheless, in the frequency range relevant in channel gating the relationship is flat.

Radial symmetry in microdomains

If we regard a channel in a small patch surrounded by, for simplicity, eight immediate neighbors in a rectangular manner, the above finding introduces a fourfold radial symmetry, because all channels can be thought to open with the same mean amplitude and stay open during a depolarization. Two different neighbors can be distinguished in this arrangement: those that make up the corners of the patch and those in-between being the nearest neighbors. We examined the gradients between the center channel and adjacent channels, asking whether gradients differ from each other, especially at the midpoints between channels. For testing this special case we adopted as closely as possible the models of Parnas et al. (1989) and Yamada and Zucker (1992), respectively. In brief, assuming channels forming a regular grid at a density of $9/\mu m^2$ (Fenwick et al., 1982), the interchannel spacing is 360 nm. Because of the fourfold symmetry the calculation can be restricted to a volume element with one 180 nm × 180 nm quadrant as outer surface. We restricted the depth of the element to 1080 nm, because this should be sufficient for short openings of channels, for which the elevation of $[Ca^{2+}]_i$ is restricted to a narrow region underneath the membrane. We used the numerical approximation given in Yamada and Zucker (1992) to solve the simple (unbuffered) diffusion equation for $[Ca^{2+}]_i$ in three dimensions. This requires the 180 × 180 × 1080 nm volume element be subdivided into small compartments. We have chosen to divide it into 6000 18-nm cubes. For short channel openings pumps and other extrusion or sequestration mechanisms should be negligible. They are therefore not included in this model. At all boundaries of the model element a zero-flux is assumed.

With this model we found gradients between the two classes of neighbors mentioned above to be nearly identical, having about the same amplitude even at the midpoints between channels. Thus, the gradients at any position along an orbit around a channel pore are zero or close to zero. We exploited this simple symmetry property of microdomains to reduce the three-dimensional diffusion problem to two dimensions. This simplification reduces computation time for a typical simulation on a workstation from ~70 to 5 min. All calculations presented below are making use of this simplification.

The simplified model

A spherical cell with N_{ch} regularly spaced identical channels can be subdivided into N_{ch} conical prisms that represent the areas of influence of a given channel. The symmetry arguments given above guarantee that there is no flux across the boundaries of such conical prisms in the case that channels are activated uniformly. Based on our simulations of diffusion in three dimensions (see above) we approximate a conical prism by an ideal cone for which the Laplacian should be given in spherical coordinates r, φ, θ by

$$\Delta = \frac{\partial^2}{\partial r^2} + \frac{2}{r}\frac{\partial}{\partial r} + \frac{1}{r^2}\left\{\frac{\partial^2}{\partial \theta^2} + \cot\theta\frac{\partial}{\partial \theta} + \frac{1}{\sin^2\theta}\frac{\partial^2}{\partial \varphi^2}\right\} \quad (3)$$

In this approximation the width of such a sector is given by one half of the angle subtended by the cone, $\theta_0 = h_{ch}/r_0$, where h_{ch} is the half-distance between two channels, and r_0 is the cell radius. We choose h_{ch} such that the area of a disk of membrane with radius h_{ch} is equal to the area per channel. Ca^{2+} enters each sector through a point source at the center of the outer surface (cell membrane), and diffuses radially along the longitudinal axis of the cone and laterally to adjacent cones. Between adjacent open Ca^{2+} channels (near h_{ch}) the lateral gradients $\partial[Ca^{2+}]/\partial\theta$ are expected to approach zero because of microdomain overlap.

Because microdomains show spherical symmetry, the gradients $\partial[Ca^{2+}]/\partial\varphi$ also should be close to zero at any location (r, φ, θ). This allows us to reduce the systems dimension by setting

$$\frac{1}{\sin^2\theta}\frac{\partial^2}{\partial \varphi^2} = 0 \quad (4)$$

in the Laplace operator, and we are left now with a two-dimensional diffusion problem.

Boundary conditions

At the boundaries $r = 0$ and $r = r_0$ we define for Ca^{2+} diffusion:

$$D\frac{\partial}{\partial r}[Ca^{2+}] = \begin{cases} \delta(\theta)J_{Ca}(t) + P_{Ca}(t) & \text{at } r = r_0 \\ 0 & \text{at } r = 0 \end{cases} \quad (5)$$

Here, $\delta(\theta)$ is a delta-distribution centered on the channel's mouth, and defines the point source for Ca^{2+} at ($r = 0$, $\theta = 0$). $J_{Ca}(t)$ is the Ca^{2+}-influx, given by

$$J_{Ca}(t) = i_{SC}(t)/2FA(r_0, \theta_0) \quad (6)$$

where $i_{sc}(t)$ is the single channel current, which is nonzero only during a depolarization, F is Faraday's constant, and $A(r_0,\theta_0)$ is the area of the membrane patch defined by the sector. $P_{Ca}(t)$ describes the active efflux by

the action of Na^+-Ca^{2+}-exchangers and Ca^{2+}-ATPases. These extrusion mechanisms were modeled as a single lumped process with Michaelis-Menten kinetics (Sala and Hernández-Cruz, 1990). To assure stability of the model for $J_{Ca}(t) = 0$ at a basal calcium level $[Ca^{2+}]_{(t)} = [Ca^{2+}]_0$, the pump term has to be counterbalanced by a constant "leak." Thus, the efflux term is given by

$$P_{Ca}(t) = -\nu_{max}[Ca^{2+}]/(K_M + [Ca^{2+}]) + \nu_{max}[Ca^{2+}]_0/(K_M + [Ca^{2+}]_0) \quad (7)$$

Inasmuch as all removal mechanisms for Ca^{2+} in chromaffin cells act on a time scale much slower than diffusional exchange, sequestration into internal stores can be neglected or mimicked by the above lumped process, respectively.

Because of the symmetry of diffusion for a uniform distribution of open channels, Ca^{2+} diffusion across the boundaries to neighboring domains is zero, resulting in

$$D\frac{\partial}{\partial\theta}[Ca^{2+}] = 0 \quad \text{at} \quad \theta = 0 \quad \text{and} \quad \theta = h_{ch}/r_0. \quad (8)$$

Assuming mass action balance for all mobile buffers, we arrive at the following boundary conditions for buffer diffusion:

$$D\frac{\partial}{\partial r}[B_m] = 0 \quad \text{at } r = 0 \quad \text{and } r = r_0,$$
$$D\frac{\partial}{\partial\theta}[B_m] = 0 \quad \text{at } \theta = 0 \quad \text{and } \theta = h_{ch}/r_0 \quad (9)$$

Initial conditions

During the time preceding a stimulus we assume $[Ca^{2+}]_i$ equilibrium. This implies the absence of gradients, and equilibrium of all buffer species with their Ca^{2+}-complexed forms:

$$[B]_0 = \frac{K_D[B_X^{total}]}{[Ca^{2+}]_{initial} + K_D} \quad (10)$$

Here $[Ca^{2+}]_{initial}$ usually is given by the resting concentration $[Ca^{2+}]_0$.

Numerical integration

The transport equations were solved numerically with standard finite difference methods. In space we discretized the sector into a series of convex shells for radial diffusion and subdivided those disks into a number of annular elements for lateral diffusion (Fig. 2 *B*). The midpoints of all volume elements $V_{j,l}$ generate a grid, where each rim-distant gridpoint $P_{j,l}$ has two neighbors $P_{j-1,l}$, $P_{j+1,l}$ in radial direction separated by straight lines of length $\Delta r_{j,l}$ and $\Delta r_{j,l+1}$ and two lateral neighbors $P_{j,l-1}$, $P_{j,l+1}$ in a distance $r_{j,l}\Delta\theta_{j,l}$ and $r_{j,l}\Delta\theta_{j,l+1}$, respectively. The $r_{j,l}$ are the radii of the $P_{j,l}$. Because steep gradients are expected near the membrane, the mesh-width was selected to be smaller there, resulting in geometrical parameters as listed in Table 1.

While diffusional exchange between adjacent volume elements ($\tau \propto \Delta r^2/D$; ~1 μs for Δr = 10 nm) and buffer reaction ($k_B^+[B]$) happens in microseconds, we were interested in modeling evolution of buffered diffusion with spatial scales $l \gg \Delta r$ and on the seconds time scale. Thus, we preferred an implicit method for the solution of the equations. Unfortunately, the equations are nonlinear due to the kinetic terms, but if the concentrations of free buffers are held fixed, the equation for $[Ca^{2+}]_i$ becomes linear. This way, we could use a modified Crank-Nicolson approximation with staggered time grids for $[Ca^{2+}]_i$ and all the buffers, respectively. Given $[Ca^{2+}]_i$ at the time step n we advanced all buffer concentrations B_X from $n - \frac{1}{2}$ to $n + \frac{1}{2}$ with a first trapezoidal rule step.

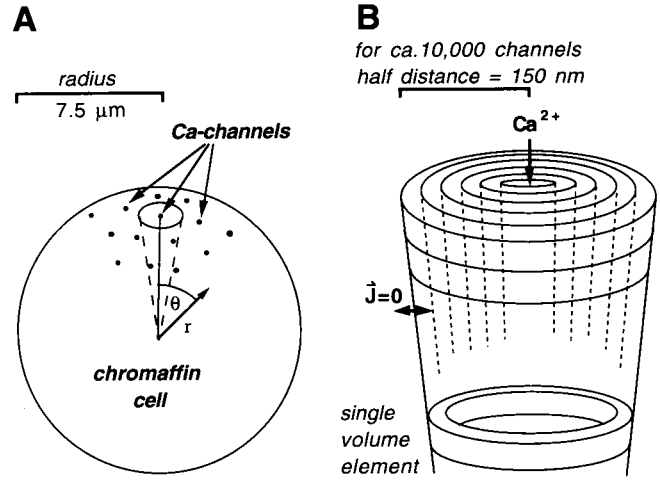

FIGURE 2 Schematic of the 2D microdomain model of buffered Ca^{2+} diffusion. (*A*) Ca^{2+} enters the spherical cell through equally spaced discrete points, from where it diffuses radially toward the cell center and laterally to adjacent channels. Because of this symmetry the calculation of diffusion can be restricted to a conical section of the sphere representing the range of influence of a given channel. At the boundary of this conical prism Ca^{2+} efflux and influx (coming from all other channels) are equal if injected currents at all point sources are the same. This condition holds, since Ca^{2+} channel flickering is reasonably fast compared to secretion (Fig. 1). (*B*) Schematic of a cone element illustrating the two-dimensional discretization.

TABLE 1 Number and size of compartments

Compartments	Δr (nm)
$V_{j,1}$ to $V_{j,10}$	10
$V_{j,11}$ to $V_{j,20}$	30
$V_{j,21}$ to $V_{j,30}$	90
$V_{j,31}$ to $V_{j,40}$	270
$V_{j,41}$ to $V_{j,45}$	700

We then used the $B_X^{n+1/2}$ to advance $[Ca^{2+}]_i$ from n to $n + 1$ with another trapezoidal rule step. This trick was used first by Hines (1984) to efficiently solve the full nonlinear Hodgkin-Huxley cable equations. If we disregard for the moment the θ space dimension, the mathematical problem involves inversion of an m by m matrix, with m being the number of compartments in radial direction for each species at each time step. This can be performed easily, as these matrices are sparse and tridiagonal.

If this scheme is simply extended for the θ dimension, the resulting matrices will still be sparse, but no longer tridiagonal. Thus, its solution would be very time-consuming. For this reason we preferred the alternating-direction implicit method (see, e.g., Ames, 1977): each time step was divided into two steps of size $h_{1/2} \equiv h/2$, and a different dimension was implicitly treated in each substep. The system maintained its tridiagonal structure and remained second-order correct in time like the Crank-Nicolson scheme for one dimension.

The validity of the model was tested for conditions where analytical solutions were available. For one mobile buffer and a large distance between channels (1.3 μm) a pseudosteady state is obtained in <1 ms. Such simulated profiles of $[Ca^{2+}]_i$ versus distance were compared with the predictions of an analytical steady-state solution for a single point source in an infinite plane (Neher, 1986; Stern, 1992). For the borderline case of one discrete element in θ direction the two-dimensional model must give, for geometrical reasons, the same solution as a shell model (Connor and Nikolakopoulou, 1982; Sala and Hernández-Cruz, 1990). This was exploited to check the model's time evolution for agreement with the data of Nowycky and Pinter (1993).

The numerical routines were written in C language, compiled and run on a Sun workstation (Sun Microsystems, Inc., Mountain View, CA). Simulated data were further processed and analyzed using IGOR (WaveMetrics, Inc., Lake Oswego, OR) and MATLAB (MathWorks, Inc., Natick, MA) on a Macintosh Quadra Computer.

Choice of parameters

Calcium channels, calcium, and calcium extrusion

For a cell with a diameter of 15 μm the depolarization-induced whole-cell Ca^{2+} current (i_{wc}) typically is 500 pA. From noise analysis the single channel current i_{sc} was estimated to ~30 fA at +10 mV for 1 mM external $[Ca^{2+}]_i$ (Fenwick et al., 1982). The half-activation potential is ~−3 mV. Thus, the open probability p_o must be well above 50% at +10 mV. Assuming, for 2 mM external $[Ca^{2+}]_i$, 50 fA for the single channel current and an open probability of 90%, we arrive at $N_{ch} \approx 11{,}000$ channels. Based on noise analysis Fenwick et al. (1982) estimated the channel density at 5–15 channels per μm^2. This gives 4,000–11,000 channels for the model cell (in contrast ~20,000 channels were estimated by Artalejo et al., 1992). The relevant parameter in the model is the half-distance between two channels, which amounts to 150 nm for 10,000 channels. The single channel current is derived from the half-distance and the whole cell current.

The diffusion coefficient of Ca^{2+} ions in water is 600 $\mu m^2/s$ (Robinson and Stokes, 1955). Because of tortuosity and viscosity the values for small ions in the cytoplasm are actually smaller by a factor of 2 to 3 (Kushmerick and Podolsky, 1969). In buffer-free oocyte cytoplasm the diffusion coefficient for Ca^{2+} ions was measured to 220 $\mu m^2/s$ (Allbritton et al., 1992). This figure was chosen in all simulations.

Ca^{2+} extrusion was modeled as one lumped process according to Sala and Hernández-Cruz (1990). Their value of 2 pmol/s for the maximal velocity V_{max} did not fit our Fura-2 measurements, thus a slightly higher value (5 pmol/cm^2/s) was chosen.

Endogenous buffers

The total Ca^{2+} binding ratio κ of endogenous buffers (the ratio of bound to free $[Ca^{2+}]_i$ changes) in chromaffin cells is, on average, 41 (Zhou and Neher, 1993). Often the ratio decreased during the course of an experiment by up to 25%. Thus in the present study the endogenous buffers were lumped into an immobile buffer with $\kappa = 31$, and a slowly mobile buffer with $\kappa = 10$ and a diffusion constant of 15 $\mu m^2/s$. The latter was estimated according to the washout time constant. Both mobile and immobile buffers have low Ca^{2+} affinity, so their K_D appears to be >5 μM. A value of 10 μM was chosen throughout all simulations.

Calbindin is a Ca^{2+} binding protein in neurons that is believed to play a role in Ca^{2+} buffering (Heizmann and Braun, 1992). Calbindin-D9k has two binding sites with on-rates of $\sim k_f = 2 \times 10^9\ M^{-1}s^{-1}$ (Forsén et al., 1988). The affinities for Ca^{2+} are highly pH-sensitive and are reduced 5- to 10-fold in the presence of 2 mM $[Mg^{2+}]$ (Cox et al., 1990). Thus under physiological conditions the apparent on-rate should be of the order of $5 \times 10^8\ M^{-1}s^{-1}$, a value also chosen in many other simulations (Gamble and Koch, 1987, Gold and Bear, 1994). We used this value for all endogenous buffers.

Exogenous buffers

MgATP typically is added to the internal solution in an experiment at a concentration of 2 mM. Most of the ATP is bound to Mg^{2+} due to its high affinity. Given a pK value of 4.06 (Martell and Smith, 1977) and ~1 mM free $[Mg^{2+}]$ (total concentration in the pipette solution being 3 mM), the actual free [ATP] should be only 0.17 mM. Thus, the on-rate for Ca^{2+} and the K_D should be scaled by a factor of ~11.8 to yield the effective kinetic constants for Ca^{2+} complexation in the presence of 3 mM total $[Mg^{2+}]$.

The parameters for all other exogenous buffers used in some experiments are taken from the literature as indicated in Table 2.

Secretion model

Secretion is described by means of the kinetic model from Heinemann et al. (1994), which is based on caged-Ca^{2+} experiments. The slower steps in that model (*A* and *A*1), which serve to refill a pool of docked and release-ready granules (pool *B*), are neglected, since we restrict our analysis here to the subsecond time window. Secretion, then, is described as a series of three independent Ca^{2+} binding events to a postulated receptor as shown in the scheme below. Upon binding of the third Ca^{2+} ion the vesicle fuses with an intrinsic velocity represented by a single rate constant γ. The change in the size of the fused state C can be directly measured as cell capacitance (Marty and Neher, 1982). Combining capacitance measurements and amperometry to monitor secretion, Chow et al. (1996) recognized that release of catecholamines is delayed relative to fusion by ~3 ms. This finding is accommodated by introduction of an additional step in the kinetic scheme with rate δ.

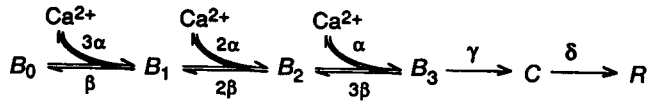

Pool B_0 varies in size between 200 and 500 fF in flash experiments (Heinemann et al., 1994) as well as for rapid trains of depolarizations (von Rüden and Neher, 1994). If not stated otherwise, a value of 250 fF was used for all simulations. The dynamics of the different states in the above scheme are described in matrix notation by

$$\frac{d\mathbf{b}}{dt} = \begin{pmatrix} -3\alpha X & \beta & 0 & 0 & 0 & 0 \\ 3\alpha X & -\beta - 2\alpha X & -2\beta & 0 & 0 & 0 \\ 0 & 2\alpha X & -2\beta - \alpha X & 3\beta & 0 & 0 \\ 0 & 0 & \alpha X & -3\beta - \gamma & 0 & 0 \\ 0 & 0 & 0 & \gamma & -\delta & 0 \\ 0 & 0 & 0 & 0 & \delta & 0 \end{pmatrix} \mathbf{b}, \tag{11}$$

where X denotes $[Ca^{2+}]_i$, α, β, γ, and δ are the rate constants of the kinetic scheme, and $\boldsymbol{b} = (B_0\ B_1\ B_2\ B_3\ C\ R)^T$ is the vector of the pool sizes of vesicles that have bound zero, one, two, or three Ca^{2+} ions (as denoted by the subscripts), have fused with the membrane, or have released their content ($\alpha = 8\ \mu M^{-1}s^{-1}$; $\beta = 105\ s^{-1}$; $\gamma = 1000\ s^{-1}$; $\delta = 330\ s^{-1}$). This set of coupled ordinary differential equations was solved numerically using a four-step Runge-Kutta routine written in IGOR macro language.

RESULTS

Two types of submembrane $[Ca^{2+}]_i$ gradients during depolarizations

To demonstrate the influence of an exogenous mobile buffer we calculated submembrane $[Ca^{2+}]_i$ gradients at the end of 20 ms depolarizations for various Fura-2 concentrations. These are graphically represented in Fig. 3 *A* for the case of 10,000 channels with interchannel spacings of 300 nm. Close to the channel mouth the $[Ca^{2+}]_i$ reaches, as expected, a high level of several tens of micromolar on average, irrespective of the concentration of exogenous buffers present. Here, the Ca^{2+} clearance is dominated by Ca^{2+}

TABLE 2 Parameters used for simulations

Symbol	Definition	Standard value	Comment
Geometry			
r_0	cell radius	7.5 μm	corresponds to 7 pF cell, also used by Nowycky and Pinter, 1993
h_{ch}	half-distance between open channels	0.15 μm	see text
Calcium			
i_{wc}	whole-cell current	500 pA	~70 pA/pF, value used by Nowycky and Pinter, 1993
$[Ca^{2+}]_0$	basal calcium concentration	0.1 μM	
D_{Ca}	diffusion constant for free calcium in cytoplasm	220 $\mu m^2 s^{-1}$	Allbritton et al., 1992
Calcium extrusion			
V_{max}	maximum velocity of transport	5 pmol $cm^{-2} s^{-1}$	the value of 2 pmol/s used by Sala and Hernández-Cruz (1990) was too small to fit our experimental data of the decay of $[Ca^{2+}]_i$
K_M	Michaelis-Menten constant	0.83 μM	Sala and Hernández-Cruz, 1990
Endogenous buffers			Zhou and Neher, 1993
Fixed buffer			
$[B_f]$	total concentration	310 μM	conc. and affinity were chosen, so that $\kappa = 31$
K_D	dissociation constant	10 μM	
k_{on}	forward binding rate	5×10^8 $M^{-1} s^{-1}$	~2×10^9 for calbindin (Forsén et al. 1988), divided by 4 to correct for Mg^{2+}; value used in several model studies: Gold and Bear, 1994; Gamble and Koch, 1987
Poorly mobile buffer			
$[B_m]$	total concentration	100 μM	conc. and affinity were chosen, so that $\kappa = 10$
K_D	dissociation constant	10 μM	
k_{on}	forward binding rate	5×10^8 $M^{-1} s^{-1}$	see fixed buffer
D_m	diffusion constant	15 $\mu m^2 s^{-1}$	Zhou and Neher, 1993
Exogenous buffers			
Fura-2			
[Fura-2]	total concentration	100 μM	conc. used in experiments
K_D	dissociation constant	0.24 μM	apparent value, as determined routinely to calibrate Fura-2
k_{on}	forward binding rate	5×10^8 $M^{-1} s^{-1}$	Jackson et al., 1987 Kao and Tsien, 1988
D_{Fura}	diffusion constant	50 $\mu m^2 s^{-1}$	Timmerman and Ashley, 1986
MgATP			Martell and Smith, 1977
[MgATP]	total concentration	2 mM	conc. used in experiments
K_D	dissociation constant	2.3 mM	K_D for ATP multiplied by 11.8 to correct for Mg^{2+}
k_{on}	forward binding rate	5×10^8 $M^{-1} s^{-1}$	$>10^9$, corrected for Mg^{2+}
D_{ATP}	diffusion constant	200 $\mu m^2 s^{-1}$	value in water of a 500-Da molecule, divided by 2 to correct for viscosity
EGTA			
[EGTA]	total concentration	1 mM	
K_D	dissociation constant	0.15 μM	
k_{on}	forward binding rate	10^7 $M^{-1} s^{-1}$	Neher, 1986
D_{EGTA}	diffusion constant	200 $\mu m^2 s^{-1}$	value in water of a 500-Da molecule, divided by 2 to correct for viscosity

diffusion rather than buffering (Neher, 1986; Stern, 1992). $[Ca^{2+}]_i$ is falling off along steep gradients in all directions, with their steepness reflecting the effectiveness of buffers at competing with diffusion as radius increases. Between channels, these microdomains of high $[Ca^{2+}]_i$ overlap giving rise to a second type of gradient, pointing toward the center of the cell. Subsequently, these will be called *submembrane domains*, as opposed to microdomains. In contrast to microdomains, these gradients are rather shallow; their amplitude, as well as their steepness, critically depend on the buffer conditions. For standard buffering conditions (i.e., with 100 μM Fura-2 included) the $[Ca^{2+}]_i$ between channels reaches ~1.9 μM, as opposed to 4.8 μM in the absence of Fura-2 and 0.31 μM in the presence of 500 μM Fura-2. Submembrane domains reach peak values at least an order of magnitude smaller than those of microdomains, and are much more sensitive to buffers both in amplitude and steepness.

Dissipation of submembrane $[Ca^{2+}]_i$ gradients

The right side of Fig. 3 represents the corresponding $[Ca^{2+}]_i$ transients underneath the membrane at various distances from a channel pore. During a depolarization $[Ca^{2+}]_i$ rises within microseconds to steady-state levels of several tens of micromolar; $[Ca^{2+}]_i$ rises more slowly the further in distance from the channel. This reflects the increasing diffu-

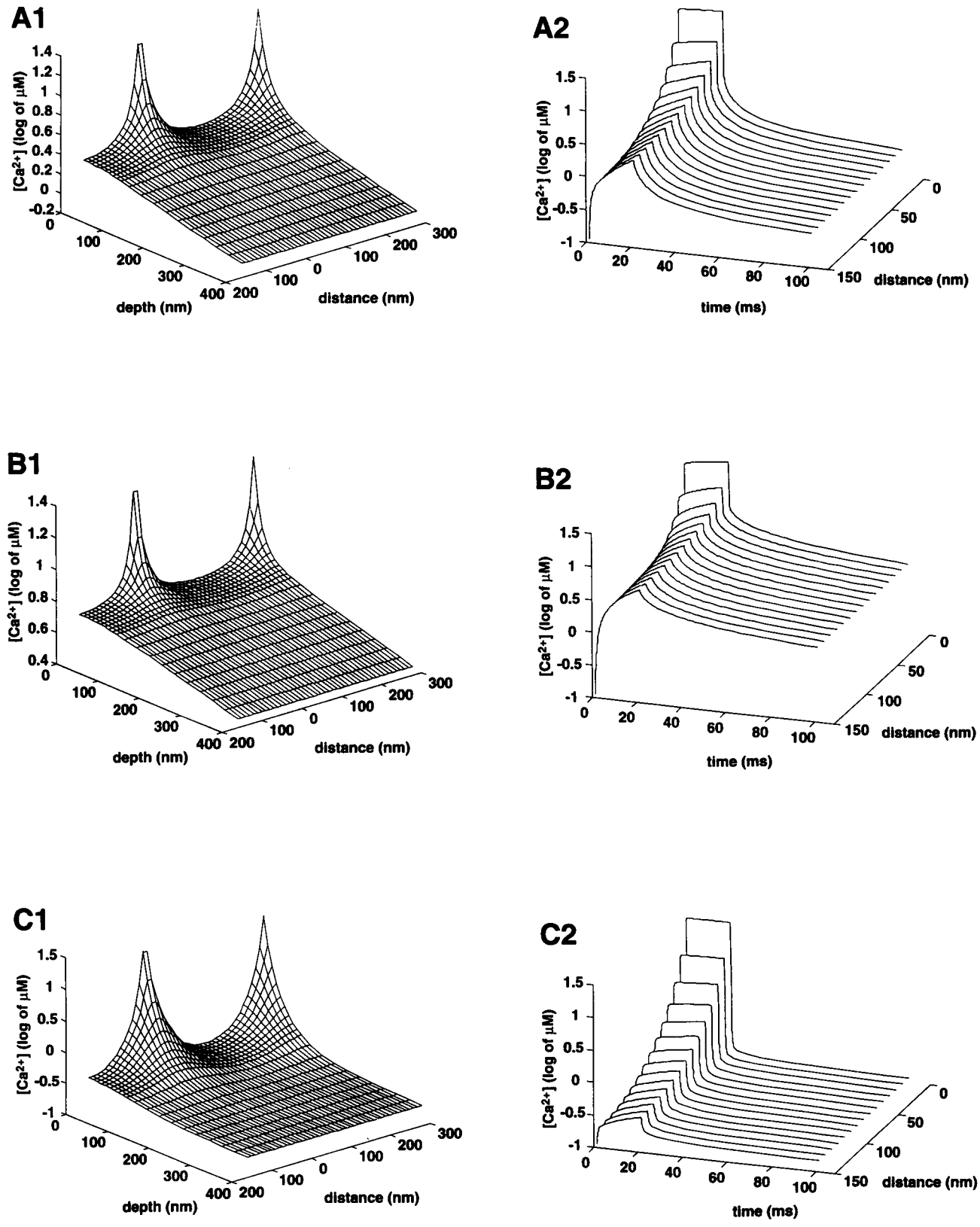

FIGURE 3 Two types of submembrane $[Ca^{2+}]_i$ gradients during depolarizations. Simulations of submembrane $[Ca^{2+}]_i$ under various Fura-2 concentrations. 10,000 Ca^{2+} channels have been assumed with an interchannel spacing of 300 nm. On the left-hand side submembrane gradients at the end of a 20-ms depolarization are shown. On the right-hand side the corresponding submembrane time courses are plotted. Submembrane domains reach peak values at least an order of magnitude smaller than those of microdomains and are much more sensitive to buffers both in amplitude and steepness. (*A*) Standard buffering conditions (i.e., with 100 µM Fura-2 included). (*B*) No added Fura-2. (*C*) 500 µM Fura-2.

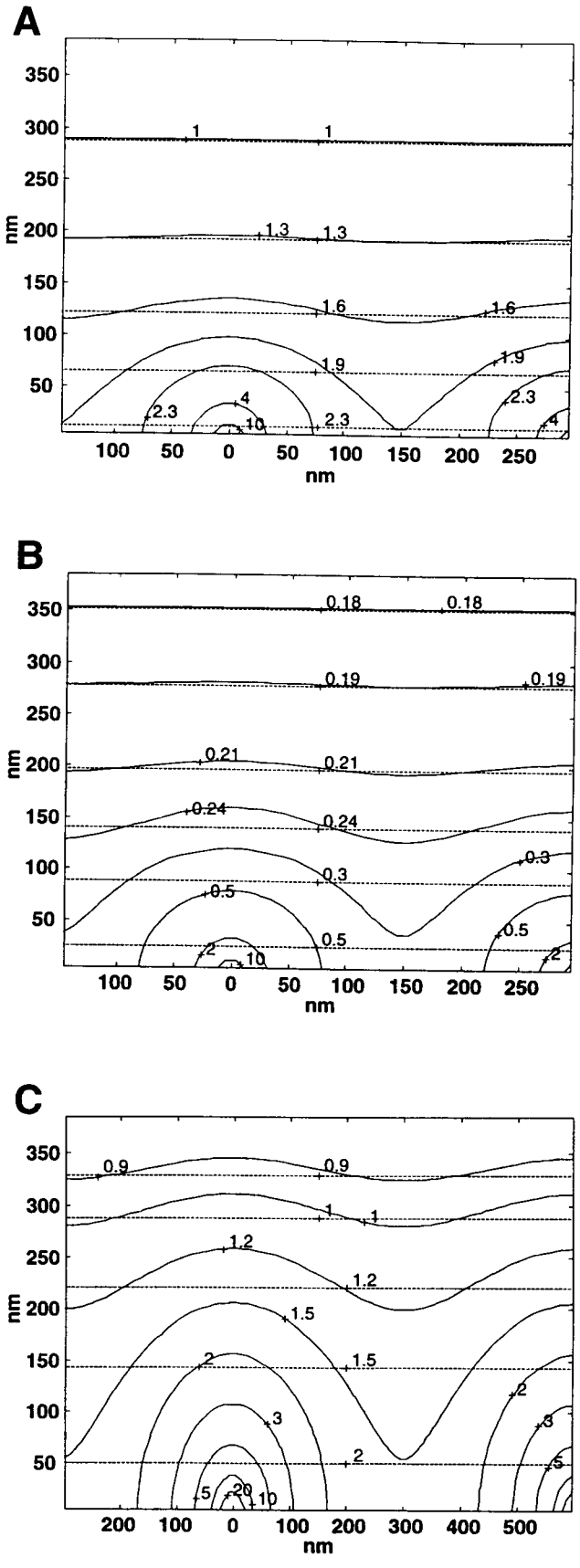

FIGURE 4 Comparison of the microdomain model with the shell model. If Ca^{2+} entry is not restricted to discrete points, but allowed to enter uniformly everywhere on the cell surface, the microdomain model presented here becomes a so-called shell model. Plotted are contour lines connecting points of equal concentration for a shell model (*dashed*) and a microdomain model (*solid*) for different buffering conditions at the end of a 20 ms depolarization. The abscissa is the distance along a line connecting two channels; the ordinate is the radial distance from the membrane. The concentration of the contour lines is indicated in μM. (*A*) 100 μM Fura-2 added. (*B*) 500 μM Fura-2. (*C*) Same as in (*A*), but only 2500 channels assumed (600-nm interchannel spacing).

sional distance or mean displacement $\sqrt{\overline{x^2}}$, which is correlated with time by $\overline{x^2} \propto D\tau$. During the depolarization no stationary $[Ca^{2+}]_i$ is reached. Near the channel $[Ca^{2+}]_i$ collapses extremely fast after channel closure, and reaches, within a few tens of microseconds, the $[Ca^{2+}]_i$ level that prevails in between channels. The decay time course can be approximated by a sum of many exponential terms having time constants of a few, up to several hundred, milliseconds. A multiexponential decay is also found in the absence of any buffers (data not shown). While the $[Ca^{2+}]_i$ dynamics in the microdomains are mostly determined by diffusion, buffers display a large effect on the decay characteristics of the submembrane domains, as exemplified in the simulations with varying Fura-2 concentrations in Fig. 3.

Comparison of the microdomain model with the shell model

If Ca^{2+} entry is not restricted to discrete points, but allowed to enter uniformly everywhere on the cell surface, the model presented here becomes identical to so-called shell models (Sala and Hernández-Cruz, 1990; Nowycky and Pinter, 1993). The diffusion process is completely symmetrical in all directions perpendicular to the radial direction, and concentration profiles need to be calculated only in that direction, which constitutes a large reduction in computation time. Qualitatively, the concentration time courses as obtained from microdomain models at many locations are quite similar to the time courses of the corresponding simple shell model if an appropriate shell is chosen (Fig. 4). We explored this similarity quantitatively by simulating several cases with the same buffer composition and the same total Ca^{2+} current, but distributing the Ca^{2+} influx among a varying number of channels. Fig. 5 *A* shows $[Ca^{2+}]_i$ profiles (concentration versus distance from the membrane) at midpoints between channels at the end of a 500-pA Ca^{2+} current pulse. For a very large number of channels and correspondingly very small interchannel distance the profile is identical with that of a shell model (uppermost curve in Fig. 5 *A*). The other curves represent profiles obtained with models assuming interchannel distances as indicated in the figure. We then asked the question, where in the profile of the shell model does the $[Ca^{2+}]_i$ agree with the peak of a given domain model profile (i.e., with the submembrane $[Ca^{2+}]_i$ value at a midpoint between two channels)? We plotted this "equivalent depth" as a function of interchannel half-distance in Fig. 5 *D*. It is seen that for a relatively large

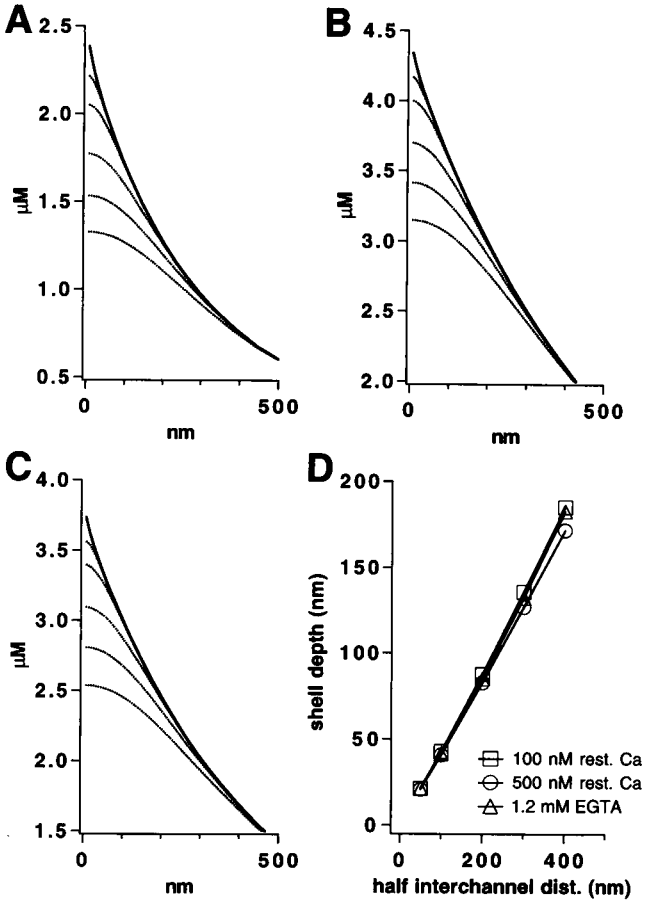

FIGURE 5 The shell model provides good estimates of the amplitude and time course of submembrane domains. (*A*) Plotted are $[Ca^{2+}]_i$ profiles along radial cross-sections at midpoints between channels at the end of a 20-ms pulse with an amplitude of 500 pA. Dotted curves correspond to simulations with interchannel distances of 100 nm, 200 nm, 400 nm, 600 nm, and 800 nm, respectively (from top to bottom). The larger the number of channels assumed, the more the profile approaches that of a shell model (*upper solid curve*). 100 μM Fura-2 are added as exogenous buffer. Resting $[Ca^{2+}]_i$ has been set to 100 nM. (*B*) Same as (*A*), but resting $[Ca^{2+}]_i$ is 500 nM. (*C*) As in (*B*), but in addition to 100 μM Fura-2, 1.2 mM EGTA have been included. (*D*) The equivalent depth, i.e., the distance from the membrane at which the $[Ca^{2+}]_i$ in a shell model equals the submembrane $[Ca^{2+}]_i$ at the midpoints between two channels in a microdomain model, is plotted as a function of interchannel half-distance.

range of interchannel distances these values are located on a straight line. Furthermore, two similar simulations with different buffer conditions gave straight lines almost identical to one another. The slope of these lines varied between 0.43 and 0.46. One can thus conclude that submembrane $[Ca^{2+}]_i$ at the midpoint between two channels can be approximated by the value given by a corresponding shell model at a depth 45% of that of the distance between the point of interest and the nearest channel. Upon investigating time courses, however, it is seen that the corresponding shell $[Ca^{2+}]_i$ transients will be slightly shifted to shorter times compared with those of the submembrane domain transients, inasmuch as the diffusional distance is shorter (by ~45%). However, for mean interchannel spacings shorter than 500 nm, as postulated for chromaffin cells, this shift is rather small, so that a shell model should be a good approximation for estimating the $[Ca^{2+}]_i$ dynamics in the submembrane domain, if the equivalent location is chosen correctly.

Comparison of back-calculated with simulated $[Ca^{2+}]_i$ time courses

In previous work we studied the time course of catecholamine release elicited by 20-ms depolarizing pulses. Based on a kinetic description of the release process and its Ca^{2+} dependence, we back-calculated the time course of $[Ca^{2+}]_i$ required at the release site for the observed response. We found resulting $[Ca^{2+}]_i$ changes to be relatively slow, and postulated that slowness was caused by diffusional delays between Ca^{2+} channels and release sites. The motivation for the present study was to provide a theoretical basis for testing this hypothesis and for estimating the diffusional distances involved.

Secretion experiments had been performed in the presence of 100 μM Fura-2 and 2 mM ATP. We included these two buffers in our simulations in addition to endogenous buffers according to Zhou and Neher (1993) (see "choice of parameters" above). Fig. 6 shows a comparison of simulated time courses for these buffering conditions in the plane of the membrane at various distances from a channel pore. The amplitude and decaying phase of the back-calculated time course (*solid line*) match very well the simulation at a distance of ~150 nm (*A*). In (*B*) the same transients are plotted after normalization to the same peak amplitude to examine the differences in time course more closely. With fewer channels (*C*) even a better fit is achieved at 300 nm, the midpoint between channels. But note that the differences in time course at distances >200 nm are rather small. This means that most of the release events are likely to be situated at a distance of ~300 nm to the nearest Ca^{2+} channel, i.e., Ca^{2+} ions have to diffuse a fair distance before they reach their target, introducing an extra delay of secretion. On the other hand, a discrepancy between simulated and back-calculated traces in the rising phase is evident. Here, the best fit is obtained for distances of ~30 nm from the channel pore (*B* and *C*). In other words, there are more fusion events at the beginning and in the early phase of a 20-ms depolarization than expected for a diffusional distance for Ca^{2+} ions of ~300 nm. As will be shown below, one way of approximating the entire back-calculated trace is to assume that the average $[Ca^{2+}]$ represents not only a temporal, but also a spatial, average, with time courses at short distances shaping the rising phase and longer distances dominating at later times.

Two functional pools of release-ready granules

For further analysis we first calculate predictions of the latency histogram according to the kinetic scheme shown

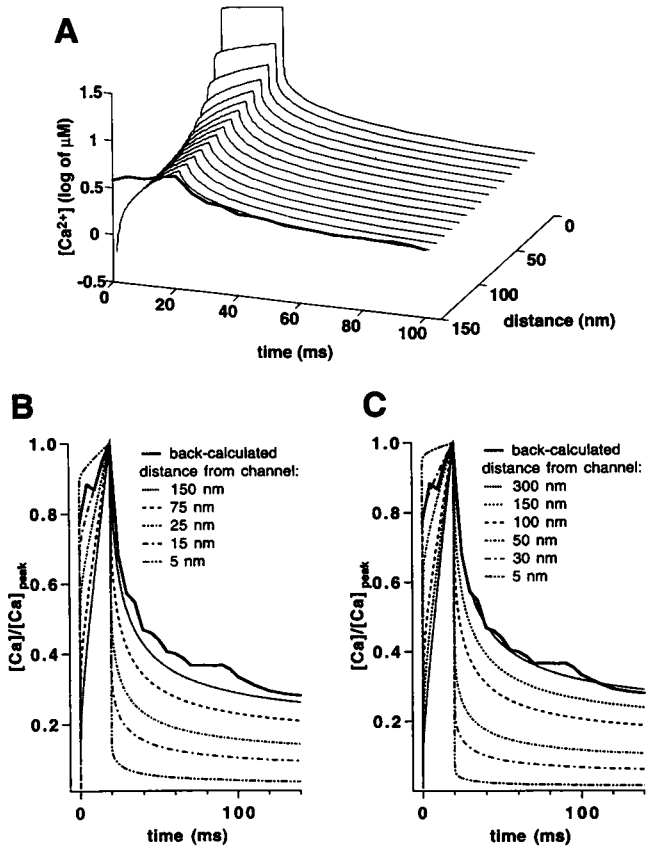

FIGURE 6 Comparison of back-calculated with simulated $[Ca^{2+}]_i$ time courses. (*A*) Simulated $[Ca^{2+}]_i$ time courses in the plane of the membrane at various distances from a channel pore are shown. Buffering conditions are as in a typical experiment (100 μM Fura-2 and 2 mM ATP). The $[Ca^{2+}]_i$ resting level has been set to 0.6 μM, which is the concentration measured in the experiments between repetitive stimuli. Superimposed is the $[Ca^{2+}]_i$ time course as inferred from combined amperometric and capacitance measurements (*thick line*). It was drawn at a position where it best matches the simulated transient in amplitude and the decaying phase (~150 nm from the channel, i.e., at the midpoint between channels, assuming 10,000 channels). The back-calculated transient differs slightly from that previously published (Chow et al., 1994). This is because the delay of release after vesicle fusion has been incorporated in the algorithm (cf. the discussion of the kinetic scheme of secretion in Methods). To achieve a better fit the whole cell current in the simulation had to be increased to 600 pA. (*B*) Simulated transients and the back-calculated $[Ca^{2+}]_i$ time course of (*A*) are plotted after normalizing all curves to the same peak amplitude to emphasize the differences in time course; 10,000 channels per cell. (*C*) With 2500 channels best agreement between experimentally inferred and simulated calcium transients is achieved at 300-nm distance (midpoint between channels).

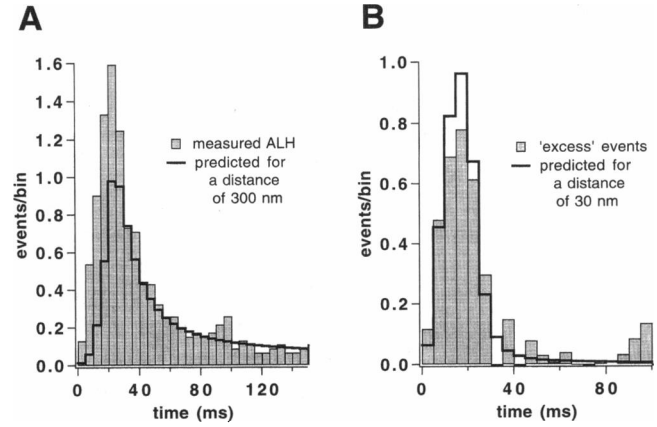

FIGURE 7 The possibility of two functional pools of release-ready granules. (*A*) Using the kinetic scheme of secretion, the amperometric latency histogram (ALH) is simulated for the hypothetical case that all release-ready granules (100) are located at a distance of 300 nm from the nearest Ca^{2+} channel (buffering conditions as in Fig. 6). Superimposed is a measured ALH under these buffering conditions (taken from Chow et al., 1994), which has been normalized to a single depolarization. For short latencies, the probability of release at the beginning of the depolarization is higher than expected for the diffusional distance of 300 nm. (*B*) Excess events from (*A*) are plotted as the "difference" histogram (*solid line*). This histogram is well fitted with a simulated ALH under the assumption that the vesicles contributing are 30 nm away from the channels (*filled histogram*). To adjust its area, ~8 vesicles have to be collocalized with channels at a distance of 30 nm (i.e., 8% of the total pool of release-ready granules).

above for the hypothetical case that all release-ready vesicles are located at a distance of 300 nm. The decaying phase of such a predicted latency histogram fits the measured histogram very well (Fig. 7 *A*). For short latencies, however, there are "excess" events in the measured histogram, i.e., the probability of release at the beginning of the depolarization is higher than expected for the diffusional distance of 300 nm. If we subtract the simulated histogram in (*A*) from the measured one, we are left with a histogram of excess events. This histogram can be well fitted under the assumption that the vesicles are 30 nm away from the channels. The total histogram is then satisfactorily reproduced if 8% of the total pool of release-ready vesicles are assumed to be collocalized with channels, at 30 nm spacing, in the simulation. Assuming a total pool of 250–500 fF (von Rüden and Neher, 1993) and assuming that the fusion of a dense core granule results in a capacitance increase of ~2.5 fF (Marty and Neher, 1982; Chow et al., 1996) this corresponds to 8–16 collocalized vesicles. The limited accuracy of the data does, of course, allow a multitude of other geometric arrangements, which would give satisfactory fits to the data.

The decay of secretion after a depolarization and its dependence on Ca^{2+} buffers

Chromaffin cells have significant amounts of endogenous fixed Ca^{2+} buffers. These fixed buffers tend to prolong submembrane $[Ca^{2+}]_i$ transients, whereas addition of mobile buffers is expected to lead to a more rapid collapse of gradients (Fig. 3). If most of the docked vesicles resided at larger diffusional distances and if the slower $[Ca^{2+}]_i$ dynamics at these distances were responsible for the slowness of secretion, one would expect that different buffer conditions will also change the secretion kinetics. We have therefore tested the effects of removing or elevating mobile Ca^{2+} buffers on the decay of the amperometric latency histograms (Chow et al., 1996). In fact, we found that increasing

the concentration of (exogenous) mobile buffer (Fig. 8 *A*, *top*), by adding EGTA (1.2 mM, κ_B = 960), reduces the decay time constant of the measured amperometric latency histogram by nearly one-half compared with standard conditions (100 μM Fura-2, 2 mM MgATP). With a pipette solution containing no diffusible Ca^{2+} buffers, we measured a very slow decay of the rate of secretion (Fig. 8 *B*, *top*). In the lower part of Fig. 8 simulations of secretion for these buffering conditions are shown. In both cases a total *B* pool of 250 fF has been assumed with 8% located at a distance of 30 nm and the majority of vesicles at 300 nm. The contributions of the "near" vesicles are shown as the shadowed part of histograms. The simulated composed histograms reproduce the experimentally found buffer effects very well. In the absence of any diffusible buffer a second slowly decaying component of secretion becomes apparent in both experiment and simulation. The onset of secretion after channel opening is delayed if compared with standard buffering conditions. In the simulation this is due to an increased contribution of secretion "far" from channels, whereas the response near to channels remains nearly unchanged (*shadowed histograms*). The disparate effects occur because buffers affect submembrane macrodomains, but barely affect microdomains. For high concentrations of mobile buffer, the far response is suppressed and most release events are triggered by microdomains, so that the overall shape of the composed histogram more closely resembles those obtained from synapses.

Trains of depolarizations and predicted responses in $[Ca^{2+}]_i$ and secretion

The simulations presented here show that complicated submembrane $[Ca^{2+}]_i$ dynamics can divide the pool of release-ready granules into functionally different subpools. In recent experiments the secretory response to rapid trains of short depolarizations has been studied in detail. Horrigan and Bookman (1994) reported the specific release of a small pool of ~10-15 readily releasable vesicles with a moderate repetitive stimulus paradigm. Only with continuing, or stronger, stimuli, a large pool of release-ready vesicles (comparable in size to what is termed *B* pool here) could be depleted. With 0.25 mM EGTA included in the patch pipette, secretion reached a plateau after depletion of the small pool, which the authors ascribed to an "immediate releasable pool." In the simulations shown in Fig. 9 *A* we tried to simulate these experiments. Plotted are time courses of

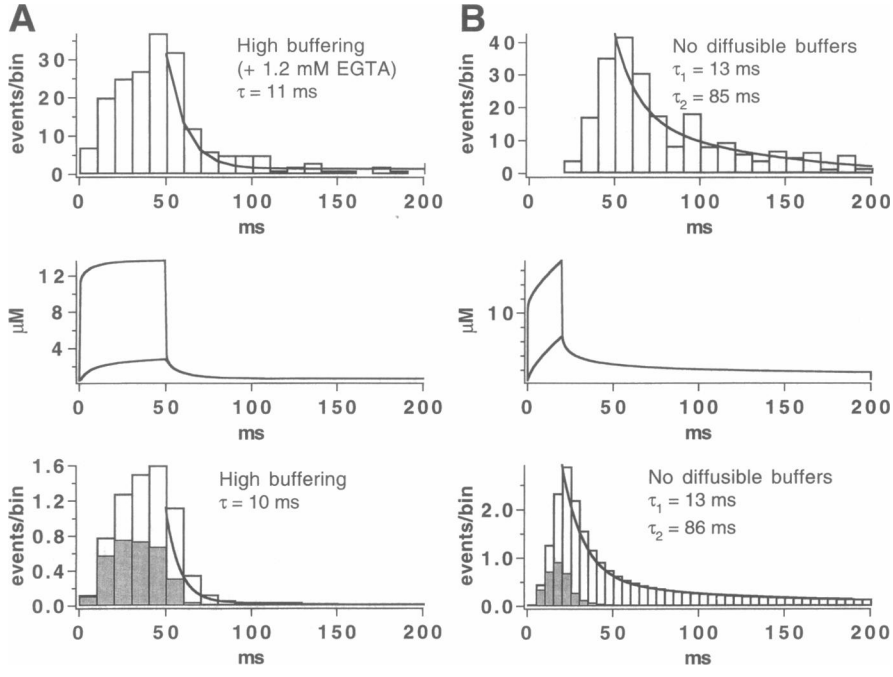

FIGURE 8 Ca^{2+} buffers shape the decay of secretion after a depolarization ends. Effects of removing or elevating mobile Ca^{2+} buffers on the decay of the ALH (experimental data replotted from Chow et al., 1996). (*A*) Top. Increasing the concentration of (exogenous) mobile buffers by adding EGTA (1.2 mM, κ_B = 960), reduces the decay time constant of the measured ALH by nearly one-half compared with standard conditions (100 μM Fura-2, 2 mM MgATP). Center. Simulations of $[Ca^{2+}]_i$ transients 30 nm and 300 nm away from the nearest channel. Buffer conditions are as in the experiments shown in (*A*). Lower panel. Simulated ALH, corresponding to the simulated $[Ca^{2+}]_i$ transients above. A total *B* pool of 250 fF has been assumed with 8% located at a distance of 30 nm and the majority of vesicles (92%) at 300 nm from the nearest Ca^{2+} channel. The contribution of the near vesicles is shown as the shadowed part of the histograms. (*B*) Top. Using a pipette solution containing no diffusible Ca^{2+} buffers, in a series of experiments the decay of secretion rate was very slow and could be better fit with two exponentials. Center. Simulations of $[Ca^{2+}]$ transients 30 nm and 300 nm away from the nearest channel for conditions as in the experiments shown in (*B*). Lower panel. Corresponding ALH. The shadowed part of the histogram reflects the contribution of the near vesicles.

$[Ca^{2+}]_i$ and capacitance for a train of 10 depolarizations (20 ms each separated by 80 ms). In addition to the endogenous fixed buffer, either 100 μM Fura-2 or 1 mM EGTA were included, as indicated. We assume an immediate releasable pool of 8 vesicles (corresponds to 8% of the total *B* pool) at a 30-nm distance from a channel, and a larger pool of 92 vesicles at a 300-nm distance. In the left panel of Fig. 9 *A* we illustrate the $[Ca^{2+}]_i$ time course at 300 nm from a channel. The right part represents the simulated secretion time course including both near and far vesicles. The responses strongly resemble what has been reported in the literature (Horrigan and Bookman, 1994; Seward and Nowycky, 1996). After depletion of the immediate releasable pool during the first two pulses, strong facilitation of the secretory response can be observed due to the onset of release at the far sites. The latter is due to incomplete clearance of Ca^{2+} after a preceding depolarization, which leads to partial buffer depletion. Thus, during the next depolarization the $[Ca^{2+}]_i$ signal is not simply added to the residual $[Ca^{2+}]_i$ in a linear fashion, but the reduced buffer capacity allows a much higher local $[Ca^{2+}]_i$. At the near sites, on the other hand, this effect is negligible, because in microdomains the $[Ca^{2+}]_i$ dynamics are dominated by diffusion and not by buffering (Fig. 3; Yamada and Zucker, 1992; Stern, 1992; Roberts, 1994). This facilitation can be suppressed in the simulations by including 1 mM EGTA, leaving only synchronous release from near secretion sites.

Simulations for brief (2 ms) action potential-like depolarizations give similar results (Fig. 9 *B*). For low stimulus frequencies or for the first depolarizations of a train, only near vesicles can be released. Because of the small size of this collocalized pool, the failure rate is very high (Fig. 9 *B*, *upper right panel*). For higher frequencies partial buffer depletion at the far release sites becomes effective after a few depolarizations, leading to facilitated fusion of far vesicles. As more and more residual Ca^{2+} is accumulated, the total secretion response becomes dominated by the more asynchronous release of far vesicles between depolarizations (Fig. 9 *B*, *lower right panel*). Exactly this behavior has been observed in isolated chromaffin cells by Zhou and

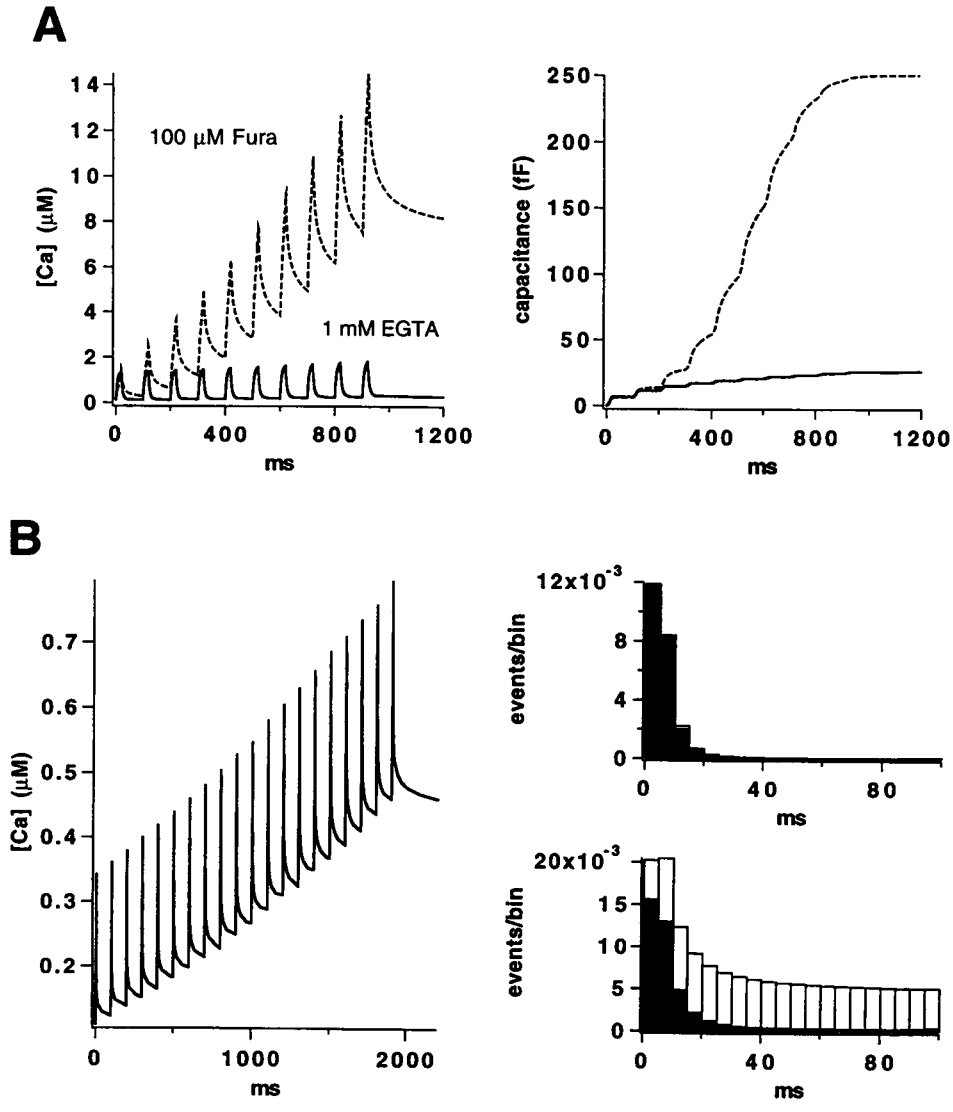

FIGURE 9 Trains of depolarizations and predicted responses in $[Ca^{2+}]_i$ and secretion. These simulations show that the complicated submembrane $[Ca^{2+}]_i$ dynamics can divide the pool of release-ready granules into functionally different subpools. (*A*) Left panel. Plotted are simulated time courses of $[Ca^{2+}]_i$ for a train of 10 depolarizations (20 ms each, separated by 80 ms). In addition to the endogenous fixed buffer, the effects of 100 μM Fura-2 or 1 mM EGTA have been simulated as indicated. Right panel. Corresponding secretion (capacitance) time courses. An immediate releasable pool of 8 vesicles (corresponds to 8% of the total *B* pool) at 30 nm distance from a channel and a large pool of 92 vesicles at 300 nm distance are assumed. (*B*) Left panel. Simulations of $[Ca^{2+}]_i$ time course at 300 nm for brief (2 ms) action potential-like depolarizations. Right panels. Simulated ALH for the first (*upper*) and the last pulse (*lower*) out of the train. Shadowed parts represent the fraction of release of near vesicles. Buffering conditions as in (*A*).

Misler (1995), when they measured the dynamics of quantal release in response to action potentials using amperometry.

DISCUSSION

In this paper we show that a variety of aspects of catecholamine secretion from chromaffin cells can be explained, if kinetic data from flash-photolysis experiments (Heinemann et al., 1994) are combined with data on Ca^{2+} buffering (Zhou and Neher, 1993) in a diffusion model. Under the simplifying assumption that Ca^{2+} channels are on average separated from release sites by ~200-300 nm, both peak and decay of the response to a short depolarizing stimulus can be described quite well. Agreement with experimental data can further be improved, if a small portion (~8%) of vesicles are assumed to be much closer to channels, at ~30 nm separation or less. In this description, the diffusion of Ca^{2+} between channels and release sites is the rate-limiting step in the overall secretory process. The aspects that are well-described include the time course of secretion in response to 20-ms pulses, its change with either adding mobile Ca^{2+} buffer or depleting Ca^{2+} buffer from the cytosol, the time course of secretion in response to trains of short depolarizations both under "native" conditions and after addition of EGTA, as well as the facilitation of the secretory response during trains of action potentials.

Two types of docked vesicles?

The model as outlined above seems to suggest a bimodal distribution of vesicles underneath the membrane. Similarly, capacitance responses to trains of depolarizations (Horrigan and Bookman, 1994) point toward a small pool of specialized vesicles. Chromaffin cells are known to contain at least two types of vesicles, small synaptic-like and large dense-core vesicles (see Thomas-Reetz and De Camilli, 1994, for review). Could the bimodal distribution thus reflect different kinetics of different vesicle types, small and large dense-core vesicles? In neurons, which contain both types of vesicles, small synaptic vesicles can fuse after arrival of a single action potential, whereas neuropeptides from large dense-core vesicles (LDCVs) are only released after trains of depolarizations, with the rate of release steeply depending on the stimulus frequency (Peng and Zucker, 1993), similar to what is found in chromaffin cells (Zhou and Misler, 1995). Using synaptosomes Verhage et al. (1991) could show that high $[Ca^{2+}]_i$ is required for neurotransmitter release, but low for neuropeptide secretion, suggesting that LDCVs are not collocalized, i.e., not docked at the active zones, where the synaptic-type vesicles are found. This scenario resembles somewhat our findings here, and in fact, the hypothesis that the collocalized fraction corresponds to synaptic-like vesicles cannot be excluded based on capacitance measurements only (Horrigan and Bookman, 1994). The pool of immediately releasable vesicles, as revealed here by analyzing amperometric latency histograms, however, cannot be attributed to small synaptic-like vesicles, unless one assumes that these small vesicles release similar amounts of oxidizable material (per vesicle) as LDCVs.

Seward and Nowycky (1996) recently made the observation that the first train of depolarizations after establishing a whole-cell patch configuration results in a secretory pattern quite different from that reported by Horrigan and Bookman (1994) or simulated in Fig. 9. Instead of facilitation, strong depression is observed, with the first 10-ms pulse of a train leading already to the fusion of at least 20 to 30 vesicles. Throughout the rest of an experiment, then, secretory responses like those in Fig. 9 are obtained. Such behavior can be described with models of diffusion and secretion as presented in this study only if one assumes that before any stimulation nearly a half of all docked vesicles reside very close to channels or are molecularly coupled. Replenishment of this special pool would have to be slow, such that it is not prominent in subsequent trains. Unfortunately, no amperometric data are available, so that it is not known whether this fast initial response reflects purely LDCV release or, in addition, some other pool of synaptic-like vesicles. Interestingly, neurohypophyseal terminals that secrete neuropeptides from LDCVs do not display this behavior (Seward and Nowycky, 1996).

Possible arrangements of channels and vesicles

The simulations presented in this paper show that the experimental latency histograms can be well described if it is assumed that the majority of vesicles is located at approximately a 300-nm distance, with a small fraction (8% of all vesicles) placed at a 30-nm distance. The latter population of vesicles is required in order to reproduce the relatively fast rising phase of latency histograms. Similarly, a small fraction (10–20%) of Ca-activated K^+ channels was recently postulated to be located close to Ca^{2+} channels in rat chromaffin cells, in order to explain time courses of outward currents under the influence of EGTA and BAPTA (Prakriya et al., 1996).

In the following, we will discuss whether such an extra population of nearby vesicles can be explained by a random distribution of vesicles and channels in which a certain number of vesicles would be close to Ca^{2+} channels by chance.

Unfortunately, the basic assumption of our model is a regular, symmetric grid of channels, such that a random distribution of both channels and granules is outside the scope of this work. It is, however, straightforward to simulate vesicles placed randomly into the surface area belonging to a cone-shaped element of our model. The probability density $p(r)$ of finding the vesicle at distance r from the channel is then proportional to the circumference of a ring at this distance, or else

$$p(r)\mathrm{d}r \propto 2\pi r\mathrm{d}r \qquad (12)$$

and the mean distance between channel and release site is

$$\bar{r} = \frac{\int_0^{h_{ch}} r 2\pi r \, dr}{\int_0^{h_{ch}} 2\pi r \, dr} = \frac{2}{3} h_{ch} \quad (13)$$

where h_{ch} is the radius of the membrane disk. With h_{ch} selected such that the area of the membrane disk ($\approx h_{ch}^2 \pi$) is the same as the mean area per channel ($1/n_0$) we obtain

$$\bar{r} = \frac{2}{3}\left(\frac{1}{\pi n_0}\right)^{1/2} \quad (14)$$

Predictions for a latency histogram are readily obtained by calculating secretory time courses according to the reaction scheme for a range of distances and superimposing these responses with weights according to $p(r)$. Such simulations show that contributions from nearby vesicles are not sufficient to result in a sufficiently fast rise in the latency histogram (data not shown). This is consistent with the fact that for a mean distance of 200 nm (the case of h_{ch} = 300 nm) only 4% of the vesicles are located within 60 nm from the closest channel. Thus, random placement of vesicles within a regular grid of channels is *not* sufficient to explain the population of nearby channels.

If, however, both channels and vesicles are placed randomly, the mean distance to the nearest channel will be significantly greater than the mean distance in the case considered above. Unfortunately, this case cannot be calculated accurately by our model, but a consideration detailed in the Appendix makes it plausible that for a random mixture the contribution of vesicles that are near channels by chance comes close to that of the postulated nearby population. Such a situation is shown schematically in Fig. 10 *A*.

It should be pointed out, though, that Monck et al. (1994) observed "hot spots" of Ca^{2+} entry in a fraction of cells, using high temporal resolution imaging techniques. These hot spots extended over one to several micrometers along the perimeter of the cells. Unfortunately, no statistics on the abundance of such hot spots and on the fraction of Ca^{2+} channels involved are available. Clustering of channels into, say, one-quarter of the surface area would not dramatically change our model predictions. If vesicles were co-clustered, but still randomly intermixed between channels within the clusters, the mean distance between channels and vesicles would be reduced by a factor of two, which does not have dramatic effects on the [Ca^{2+}]$_i$ time course of decay, as discussed above. It cannot be excluded, however, that our indications of vesicle heterogeneity are due to such inhomogeneous channel and vesicle distributions.

Importance of endogenous buffers and mean diffusional distance to channels

In our simulations we identified the slow decay of the [Ca^{2+}]$_i$ transients at the secretory sites as responsible for the slowness of secretion in chromaffin and other neuroendocrine cells. In particular, the mean distance between the fusion machinery and Ca^{2+} channels and the buffering conditions are the two critical parameters that shape the [Ca^{2+}]$_i$ transients. Changing either will result in a shift of the time course of secretion.

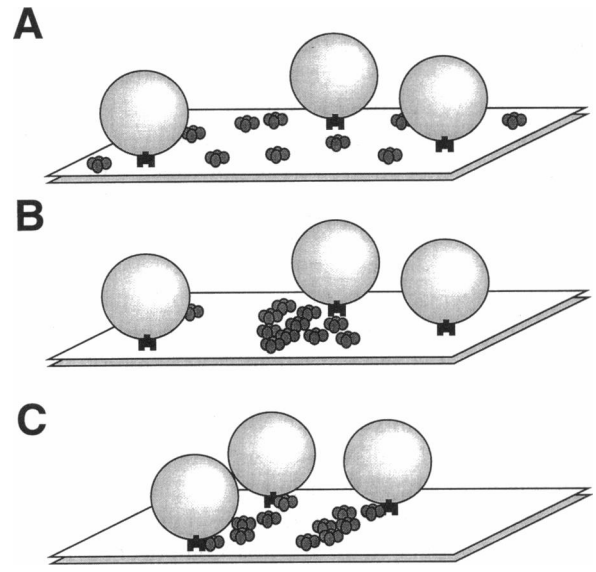

FIGURE 10 Possible arrangements of vesicles and Ca^{2+} channels in the membrane. (*A*) Random distribution of channels and vesicles. (*B*) Random distribution of vesicles and clustering of Ca^{2+} channels. (*C*) Collocalization and molecular coupling of channels and vesicles in defined areas (active zones). For discussion see text.

A key question motivating this study was whether the buffer capacity of endogenous fixed buffers would be sufficient to retard the submembrane Ca^{2+} diffusion to a degree resulting in locations underneath the membrane, where the theoretically predicted [Ca^{2+}]$_i$ time course matches the experimentally predicted one. We found that a mean distance of 200 nm for a random channel and vesicle distribution is sufficient to provide such locations. However, as simulations under varying buffering conditions show, uncertainties in our values of the endogenous buffering also imply uncertainties in our estimation of the mean diffusional distance. In particular, the distribution of endogenous fixed buffers might be inhomogenous, with higher concentrations close to the membrane. Cytoskeletal structures or the release-ready granules themselves could act as diffusion barriers, resulting in an even slower dissipation of the submembrane gradients, so that our estimation of the mean distance would be somewhat overestimated. However, even doubling of the buffer capacity of endogenous buffers results only in a small shift in the time course at a 300-nm vesicle-channel distance. The amplitude, in this case, is reduced by 35% for a 20-ms depolarization (data not shown).

Our simulations point out the importance of the diffusional distance in shaping the time course of secretion. Chromaffin cells display a fast synchronous response and a more slow asynchronous response, which is reminiscent of

the delayed response at the neuromuscular junction (Rahamimoff and Yaari, 1973) and in hippocampal neurons (Goda and Stevens, 1994). The difference is that in synapses the vast majority of vesicles fuses in the fast synchronous mode, which has been taken as an indication of collocalization. The proportion of fast versus slow release in chromaffin cells can be shifted in either direction by changing the buffer conditions. Because of the close proximity of channels to fusion sites in the active zones, buffers do not exert much of an effect in synapses except when used at very high concentrations (Adler et al., 1991). On the other hand, any manipulation that changes the relative position of channels with respect to release sites also should change the time course of secretion in synapses. Mice synapses lacking the synaptic vesicle protein synaptotagmin display a shift from a synchronous to a more asynchronous release, in that a fast component of secretion is remarkably reduced (Geppert et al., 1994). Assuming that the two components, fast and slow, of secretion found at these synapses represent parallel pathways (Goda and Stevens, 1994) this has been taken as evidence that synaptotagmin is the Ca^{2+} receptor responsible for fast Ca^{2+}-triggered vesicle fusion. However, the simulations presented in this study indicate that such a change can also be brought about by a disturbance of the morphological organization of the docking sites, if this increases the diffusional distance between channels and the fusion sites (see also Neher and Penner, 1994).

In other genetic studies in which synaptotagmin is mutated or deleted, a concomitant drop in the apparent order of the Ca^{2+} dependence can sometimes be observed (see Littleton and Bellen, 1995, for review). This has been interpreted as further evidence for synaptotagmin being the low-affinity receptor that binds Ca^{2+} in a cooperative fashion. The remaining asynchronous release with lower cooperativity thus should reflect the presence of a second, high-affinity receptor mediating a different type of slow secretion (loc. cit.). However, because of the inherent nonlinearity of buffered diffusion, a change in the apparent cooperativity concurrent to a change in distance is expected. Strength and direction of that change will depend on the buffer conditions in a particular preparation. In chromaffin cells, the apparent order of Ca^{2+} dependence during depolarizations is <2 in contrast to 3 in flash photolysis experiments (Engisch and Nowycky, 1996). This highlights the importance of understanding the submembrane $[Ca^{2+}]_i$ dynamics and buffering conditions as a prerequisite to understanding where Ca^{2+} binds and how its binding triggers fusion.

Physiological implications for stimulus-secretion coupling

This theoretical study shows that most of the experimental findings in isolated chromaffin cells can be explained assuming a random distribution of Ca^{2+} channels and fusion sites over the cell surface. Chromaffin cells in situ, however, are known to be polarized. They are innervated at one site and face blood capillaries at another site, which is presumably the secretory pole, since most of the vesicles are found there (Carmichael, 1987). Fusion sites and Ca^{2+} channels might still be distributed more or less randomly, but should be packed within a fraction of the whole surface. This would lead to a more pronounced overlap of channel domains, resulting in substantially higher submembrane $[Ca^{2+}]_i$ both near the channel pore and between channels. Thus, the mean diffusional distance would be shorter and the onset of secretion faster. In fact, Moser and Neher (1996) have found that 10–20-ms depolarizing pulses are sufficient to elicit capacitance responses from adrenal gland slices which correspond to the fusion of ~20 dense-core granules. It is therefore an open question whether the separation between channels and release sites, suggested by this study, has physiological relevance, or represents the situation in cell culture only. In case this model holds in situ, it would offer an explanation for the very much increased effectiveness of trains of action potentials compared with single action potentials in triggering catecholamine secretion (see also Zhou and Misler, 1995). If the situation described here also holds in the case of LDCV release in cells where LDCVs coexist with synaptic vesicles, it would provide a basis for differential release of vesicle content depending on the secretion-evoking pulse pattern. Evidence for such differential release has been presented for synaptosomes (Verhage et al., 1991) and for synapses between identified leech neurons in culture (Bruns and Jahn, 1995). Different spatial arrangements between channels and release sites, as illustrated in the cartoon of Fig. 10, may then be the basis of important functional differences among cellular release processes.

APPENDIX

Let $\hat{p}(r)$ denote the probability of not finding a channel within the area πr^2 around a vesicle. Then the probability of not finding a channel up to $r + \Delta r$ may be written as

$$\hat{p}(r + \Delta r) = \hat{p}(r) \cdot \tilde{p}(r, r + \Delta r) \tag{15}$$

where $\tilde{p}(r, r + \Delta r)$ is the probability of not finding the channel between r and $r + \Delta r$, given it was not found up to r, which for a random distribution with channel density n_0 is

$$\tilde{p}(r, r + \Delta r) = 1 - p(r)\Delta r = 1 - 2\pi n_0 r \Delta r \quad \text{for } \Delta r \to 0 \tag{16}$$

Combining Eqs. 15 and 16 and rearranging yields

$$\frac{\hat{p}(r + \Delta r) - \hat{p}(r)}{\Delta r} = -2\pi n_0 r \hat{p}(r) \tag{17}$$

If we now let $\Delta r \to 0$, we get the first-order differential equation

$$d\hat{p} = -2\pi n_0 r \hat{p}\, dr \tag{18}$$

which can be solved by separation of the variables. Integration then yields

$$\hat{p}(r) = e^{-\pi n_0 r^2} \tag{19}$$

Finally, the probability p of finding the nearest channel between 0 and r for

a random channel distribution is

$$p(r) = 1 - e^{-\pi n_0 r^2} \quad (20)$$

and for small r

$$p(r) \approx \pi n_0 r^2 \quad r \ll h_{ch} \quad (21)$$

Thus, the number of vesicles adjacent to channels is the same for both the regular and random channel distribution for a given channel density, but the mean distance to the nearest channel is not:

$$\bar{r} = \int_0^\infty r p(r)\, dr = \frac{1}{2} n_0^{-1/2} \quad (22)$$

We can now ask the question, how many vesicles, assuming a random distribution, would be close to channels for a mean distance of, say, 200 nm, for which we obtained a good fit for the decay of secretion in the case of a regular channel distribution? By comparing Eqs. 14 and 22 it is found that for a random distribution we have to increase the channel density by a factor of $9\pi/16$ ($\sim$1.8) to get the same mean distance as for a regular channel grid. Hence, the number of vesicles in close proximity to channels will be increased by the same factor. For a mean distance of 200 nm we expect 7% of all docked vesicles to be located within a 60-nm radius of the nearest Ca^{2+} channel, which is close to what we found to be compatible with our experimental data. Simulations of secretion in which all submembrane $[Ca^{2+}]_i$ transients have been weighted according to the probability of finding a channel at this distance from a vesicle, in fact, are hardly distinguishable from those shown in Figs. 8 and 9, where 92% of all vesicles have been assumed to reside at a 300-nm, and 8% at a 30-nm, distance. Of course, such simulations are only an approximation of a random distribution of vesicles and channels, since the $[Ca^{2+}]_i$ transients for these simulations still have been calculated assuming a regular channel grid with 600-nm interchannel spacing. However, because transients at distances >200 nm are very similar (compare transients at 150 nm and 300 nm in Fig. 6 *C*), a detailed diffusion model of a sphere with thousands of channels at random positions should also give very similar results at distances >300 nm.

We would like to thank Robert H. Chow for his advice during the course of this study and Corey Smith for helpful comments on the manuscript.

This work was supported in part by a grant from the EC Networks Program (No. CHRXCT940500).

REFERENCES

Adler, E. M., G. J. Augustine, S. N. Duffy, and M. P. Charlton. 1991. Alien intracellular calcium chelators attenuate neurotransmitter release at the squid giant synapse. *J. Neurosci.* 11:1496–1507.

Allbritton, N. L., T. Meyer, and L. Stryer. 1992. Range of messenger action of calcium ion and inositol 1,4,5-trisphosphate. *Science.* 258: 1812–1815.

Ames, W. F. 1977. Numerical Methods for Partial Differential Equations, 2nd ed. Academic Press, New York.

Artalejo, C. R., R. L. Perlman, and A. P. Fox. 1992. ω-Conotoxin GVIA blocks a Ca^{2+} current in bovine chromaffin cells that is not of the "classic" N type. *Neuron.* 8:85–95.

Augustine, G. J., M. P. Charlton, and S. J. Smith. 1985. Calcium entry and transmitter release at voltage-clamped nerve terminals of squid. *J. Physiol.* 367:163–181.

Bruns, D., and R. Jahn. 1995. Real-time measurement of transmitter release from single synaptic vesicles. *Nature.* 376:62–65.

Carmichael, S. W. 1987. Morphology and innervation of the adrenal medulla. *In* Stimulus-Secretion Coupling in Chromaffin Cells, Vol. 1. K. Rosenheck and P. Lelkes, editors. CRC Press, Boca Raton, Florida. 1–29.

Chad, J. E., and R. Eckert. 1984. Calcium domains associated with individual channels can account for anomalous voltage relations of Ca-dependent responses. *Biophys. J.* 45:993–999.

Chow, R. H., J. Klingauf, C. Heinemann, R. S. Zucker, and E. Neher. 1996. Mechanisms determining the time course of secretion in neuroendocrine cells. *Neuron.* 16:369–376.

Chow, R. H., J. Klingauf, and E. Neher. 1994. Time course of Ca^{2+} concentration triggering exocytosis in neuroendocrine cells. *Proc. Natl. Acad. Sci. U.S.A.* 91:12765–12769.

Chow, R. H., L. von Rüden, and E. Neher. 1992. Delay in vesicle fusion revealed by electrochemical monitoring of single secretory events in adrenal chromaffin cells. *Nature.* 356:60–63.

Connor, J. A., and G. Nikolakopoulou. 1982. Calcium diffusion and buffering in nerve cytoplasm. *Lect. Math. Sci.* 15:79–101.

Cox, J. A., M. Milos, and J. P. MacManus. 1990. Calcium- and magnesium-binding properties of oncomodulin. *J. Biol. Chem.* 265: 6633–6637.

Engisch, K. L., and M. C. Nowycky. 1996. Calcium dependence of large dense-cored vesicle exocytosis evoked by calcium influx in bovine adrenal chromaffin cells. *J. Neurosci.* 16:1359–1369.

Fenwick, E. M., A. Marty, and E. Neher. 1982. Sodium and calcium channels in bovine chromaffin cells. *J. Physiol.* 331:599–635.

Fogelson, A. L., and R. S. Zucker. 1985. Presynaptic calcium diffusion from various arrays of single channels. Implications for transmitter release and synaptic facilitation. *Biophys. J.* 48:1003–1017.

Forsén, S., S. Linse, E. Thulin, B. LindegÅrd, S. R. Martin, P. M. Bayley, P. Brodin, and T. Grundström. 1988. Kinetics of calcium binding calbindin mutants. *Eur. J. Biochem.* 177:47–52.

Gamble, E., and C. Koch. 1987. The dynamics of free calcium in dendritic spines in response to repetitive synaptic input. *Science.* 236:1311–1315.

Geppert, M., Y. Goda, R. E. Hammer, C. Li, T. W. Rosahl, C. F. Stevens, and T. C. Südhof. 1994. Synaptotagmin I: a major Ca^{2+} sensor for transmitter release at a central synapse. *Cell.* 79:717–727.

Goda, Y., and C. F. Stevens. 1994. Two components of transmitter release at a central synapse. *Proc. Natl. Acad. Sci. U.S.A.* 91:12942–12946.

Gold, J. I., and M. F. Bear. 1994. A model of dendritic spine Ca concentration exploring possible bases for a sliding synaptic modification threshold. *Proc. Natl. Acad. Sci. U.S.A.* 91:3941–3945.

Heidelberger, R., C. Heinemann, E. Neher, and G. Matthews. 1994. Calcium dependence of the rate of exocytosis in a synaptic terminal. *Nature.* 371:513–515.

Heinemann, C., R. H. Chow, E. Neher, and R. S. Zucker. 1994. Kinetics of the secretory response in bovine chromaffin cells following flash photolysis of caged Ca^{2+}. *Biophys. J.* 67:546–2557.

Heizmann, C. W., and K. Braun. 1992. Changes in Ca-binding proteins in human neurodegenerative disorders. *TINS.* 15:259–264.

Hines, M. 1984. Efficient computation of branched nerve equations. *Int. J. Bio-Medical Computing.* 15:69–76.

Horrigan, F. T., and R. J. Bookman. 1994. Releasable pools and the kinetics of exocytosis in rat adrenal chromaffin cells. *Neuron.* 13: 1119–1129.

Jackson, A. P., M. P. Timmermann, C. R. Bagshaw, and C. C. Ashley. 1987. The kinetics of calcium binding to Fura-2 and indo-1. *FEBS Lett.* 216:35–39.

Kao, J. P. Y., and R. Y. Tsien. 1988. Ca^{2+} binding kinetics of Fura-2 and azo-1 from temperature-jump relaxation measurements. *Biophys. J.* 53: 635–639.

Kushmerick, M. J., and R. J. Podolsky. 1969. Ionic mobility in muscle cells. *Science.* 166:1297–1298.

Littleton, J. T., and H. J. Bellen. 1995. Synaptotagmin controls and modulates synaptic-vesicle fusion in a Ca-dependent manner. *Trends Neurosci.* 18:177–183.

Llinas, R., I. Z. Steinberg, and K. Walton. 1981. Relationship between presynaptic calcium current and postsynaptic potential in squid giant synapse. *Biophys. J.* 33:323–351.

Martell, A. E., and R. M. Smith. 1977. Critical Stability Constants. Vol. 3: Other Organic Ligands. Plenum, New York.

Marty, A., and E. Neher. 1982. Discrete changes of cell membrane capacitance observed under conditions of enhanced secretion in bovine adrenal chromaffin cells. *Proc. Natl. Acad. Sci. U.S.A.* 79:6712–6716.

Monck, J. R., I. M. Robinson, A. L. Escobar, J. L. Vergara, and J. M. Fernandez. 1994. Pulsed laser imaging of rapid Ca^{2+} gradiens in excitable cells. *Biophys. J.* 67:505–514.

Moser, T., and E. Neher. 1996. Rapid exocytosis in single chromaffin cells recorded from adrenal slices. *Biophys. J.* 70:A85.

Neher, E. 1986. Concentration profiles of intracellular calcium in the presence of a diffusible chelator. *Exp. Brain Res.* 14:80–96.

Neher, E., and G. J. Augustine. 1992. Calcium gradients and buffers in bovine chromaffin cells. *J. Physiol.* 450:273–301.

Neher, E., and R. Penner. 1994. Mice sans synaptotagmin. *Nature.* 372: 316–317.

Neher, E., and R. S. Zucker. 1993. Multiple calcium-dependent processes related to secretion in bovine chromaffin cells. *Neuron.* 10:21–30.

Nowycky, M. C., and M. J. Pinter. 1993. Time courses of calcium and calcium-bound buffers following calcium influx in a model cell. *Biophys. J.* 64:77–91.

O'Sullivan, A. J., T. R. Cheek, R. B. Moreton, M. J. Berridge, and R. D. Burgoyne. 1989. Localization and heterogeneity of agonist-induced changes in cytosolic calcium concentration in single bovine adrenal chromaffin cells from video imaging of fura-2. *EMBO J.* 8:401–411.

Parnas, H., G. Hovav, and I. Parnas. 1989. Effect of Ca^{2+} diffusion on the time course of neurotransmitter release. *Biophys. J.* 55:859–874.

Peng, Y. Y., and R. S. Zucker. 1993. Release of LHRH is linearly related to the time integral of presynaptic Ca2+ elevation above a threshold level in bullfrog sympathetic ganglia. *Neuron.* 10:465–473.

Prakriya, M., C. R. Solaro, and C. J. Lingle. 1996. $[Ca^{2+}]_i$ elevations detected by BK channels during Ca^{2+} influx and muscarine-mediated release of Ca^{2+} from intracellular stores in rat chromaffin cells. *J. Neurosci.* 16:4344–4359.

Rahamimoff, R., and Y. Yaari. 1973. Delayed release of transmitter at the frog neuromuscular junction. *J. Physiol.* 228:241–257.

Roberts, W. M. 1994. Localization of calcium signals by a mobile calcium buffer in frog saccular hair cells. *J. Neurosci.* 14:3246–3262.

Robinson, R. A., and R. H. Stokes. 1955. Electrolyte Solutions. Butterworths, London.

Sala, F., and A. Hernández-Cruz. 1990. Calcium diffusion modelling in a spherical neuron: relevance of buffering properties. *Biophys. J.* 57: 313–324.

Schroeder, T. J., J. A. Jankowski, J. Senyshyn, R. W. Holz, and R. M. Wightman. 1994. Zones of exocytotic release on bovine adrenal medullary cells in culture. *J. Biol. Chem.* 269:17215–17220.

Seward, E. P., and M. C. Nowycky. 1996. Kinetics of stimulus-coupled secretion in dialyzed bovine chromaffin cells in response to trains of depolarizing pulses. *J. Neurosci.* 16:553–562.

Simon, S. M., and R. R. Llinás. 1985. Compartmentalization of the submembrane calcium activity during calcium influx and its significance in transmitter release. *Biophys. J.* 48:485–498.

Stern, M. D. 1992. Buffering of calcium in the vicinity of a channel pore. *Cell Calcium.* 13:183–192.

Thomas, P., J. G. Wong, A. K. Lee, and W. Almers. 1993. A low affinity Ca^{2+} receptor controls the final steps in peptide secretion in pituitary melanotrophs. *Neuron.* 11:93–104.

Thomas-Reetz, A. C., and P. De Camilli. 1994. A role for synaptic vesicles in non-neuronal cells: clues from pancreatic beta cells and from chromaffin cells. *FASEB J.* 8:209–216.

Timmerman, M. P., and C. C. Ashley. 1986. Fura-2-diffusion and its use as an indicator of transient free calcium changes in single striated muscle cells. *FEBS Lett.* 209:1–8.

Verhage, M., H. T. McMahon, W. E. Ghijsen, F. Boomsma, G. Scholten, V. M. Wiegant, and D. G. Nicholls. 1991. Differential release of amino acids, neuropeptides, and catecholamines from isolated nerve terminals. *Neuron.* 6:517–524.

von Gersdorff, H., and G. N. Matthews. 1994. Dynamics of synaptic vesicle fusion and membrane retrieval in synaptic terminals. *Nature.* 367:735–739.

von Rüden, L., and E. Neher. 1993. A Ca-dependent step in the release of catecholamines from adrenal chromaffin cells. *Science.* 262:1061–1065.

Yamada, W. M., and R. S. Zucker. 1992. Time course of transmitter release calculated from simulations of a calcium diffusion model. *Biophys. J.* 61:671–683.

Zhou, Z., and S. Misler. 1995. Action potential-induced quantal secretion of catecholamines from rat adrenal chromaffin cells. *J. Biol. Chem.* 270:3498–3505.

Zhou, Z., and E. Neher. 1993. Mobile and immobile calcium buffers in bovine adrenal chromaffin cells. *J. Physiol.* 469:245–273.